Front. Struct. Civ. Eng. 2022, 16(11): 1424–1435
https://doi.org/10.1007/s11709-022-0870-9

RESEARCH ARTICLE

Numerical investigation of the influence of casting techniques on fiber orientation distribution in ECC

Chung Nguyen VAN[a], Hai TRAN THANH[b,c*], Thuc Nhu NGUYEN[b], Jianchun LI[b]

[a] *Faculty of Civil Engineering, Ho Chi Minh City University of Technology and Education, Ho Chi Minh 721400, Vietnam*
[b] *School of Civil and Environmental Engineering, University of Technology Sydney, Sydney, NSW 2007, Australia*
[c] *School of Civil Engineering, Hue Industrial College, Hue 49120, Vietnam*
[*] *Corresponding author. E-mail: Hai.Tran@uts.edu.au*

ABSTRACT Engineered cementitious composites (ECC), also known as bendable concrete, were developed based on engineering the interactions between fibers and cementitious matrix. The orientation of fibers, in this regard, is one of the major factors influencing the ductile behavior of this material. In this study, fiber orientation distributions in ECC beams influenced by different casting techniques are evaluated via numerical modeling of the casting process. Two casting directions and two casting positions of the funnel outlet with beam specimens are modeled using a particle-based smoothed particle hydrodynamics (SPH) method. In this SPH approach, fresh mortar and fiber are discretized by separated mortar and fiber particles, which smoothly interact in the computational domain of SPH. The movement of fiber particles is monitored during the casting simulation. Then, the fiber orientations at different sections of specimens are determined after the fresh ECC stops flowing in the formwork. The simulation results show a significant impact of the casting direction on fiber orientation distributions along the longitudinal wall of beams, which eventually influence the flexural strength of beams. In addition, casting positions show negligible influences on the orientation distribution of fibers in the short ECC beam, except under the pouring position.

KEYWORDS ECC, fiber orientation distribution, casting direction, casting position

1 Introduction

Engineered cementitious composites (ECC) are materials exhibiting high tensile ductility compared to conventional concrete through optimizing the micro-mechanical interactions between short-random fibers and cementitious matrix. For this reason, the matrix of ECC contains only sands, cementitious materials, and no coarse aggregates [1]. These interactions determine the fiber-bridging strength, which limits the crack width of ECC to normally less than 60 μm [2]. The tensile strain-hardening behavior of ECC is achieved through the steady formation of multiple flat cracks at different defect zones in its matrix. In other words, this unique property of ECC is governed by the fiber-bridging behavior at its cracked planes [3,4].

In recent decades, extensive efforts have been made to understand the influencing factors on the efficiency of bridging fibers in ECC. Consequently, fiber orientation and distribution at cracked planes have been recognized as the two vital factors governing fiber-bridging behavior [5,6]. Fibers should be well distributed, to ensure consistency for bearing stress at different crack planes [7]. The orientation of a fiber determines its ultimate strength when bearing stress [8,9]. The efficiency of fibers in bearing stress at a crack plane released by the matrix thus strongly depends on the number of intersected fibers and their orientation at that plane [10,11]. In this regard, it is desirable to improve the fiber dispersion and understand factors affecting fiber orientation in ECC elements.

For a number of fiber-reinforced cement-based materials owning self-compacting or flowable properties, experimental studies have indicated that fiber orientation might be affected by formwork geometry and casting flows [12]. Different casting techniques have been performed to investigate their influences on rigid steel

Article history: Received Dec 25, 2021; Accepted May 29, 2022

fiber orientation distribution in beam specimens [13,14]. On the other hand, Kanakubo et al. [5] used a water glass solution to simulate two casting directions of the same size of ECC specimens using flexible synthetic fibers. The results of fiber orientation evaluation have illustrated the effectiveness of casting directions on fibers orientation in ECC specimens. In the later work of Ding et al. [10], three groups of ECC beams were cut from a slab in different directions with respect to the casting direction, i.e., parallel, perpendicular and diagonal directions. The "parallel" beams attained a greater degree of smaller orientation of fibers with the longitudinal direction and thus achieved higher tensile stress-strain behavior than that of in "perpendicular" and "diagonal" beams. This observation emphasized that understanding the influence of casting techniques on fiber orientation is vitally important, especially for structural members such as beams or slabs [15,16]. However, it is worth noting that observation and determination of fiber orientation in the above-mentioned experimental studies required image processing and analysis procedures, which are time-consuming and expensive. Moreover, in the experimental approach, the variation of fiber orientation distribution in the fresh mixture at the beginning of castings might also cause the dissimilarity of fiber orientations in different specimens of the hardened concrete.

Due to the above-mentioned limitations of experimental approach, numerical models have been developed to provide an alternative approach to study the flow characteristics of flowable fiber reinforced cement-based materials and to investigate distribution and orientation of fibers [17–20]. In these models, fibers are typically simulated either as rigid bodies represented by two-end particles for steel fibers [19,21] or as bendable bodies represented by interconnected particles for synthetic fibers [20]. The computational domains of fresh mixes are discretized into sets of particles, then approximately solved using Lattice Boltzmann [22] or Smoothed Particle Hydrodynamics (SPH) [17,20] methods. The introduction of fibers into concrete mixes increases the viscosity of fresh concrete. Fiber particles are simply considered as passive markers, which move and orient according to the motion of fresh mixes. With this consideration, Thanh et al. [23] developed and validated a 3D model to simulate the flow of fresh and flowable ECC. This approach has an advantage of monitoring the movement of fibers to provide a practical understanding of the distribution and orientation of fibers in structural elements [24]. The outcome is important in optimizing the casting technique to achieve the anticipated fiber orientation for improving the material performance in ECC structural elements.

Accordingly, the effect of casting techniques on the orientation distribution of synthetic fiber in ECC beams is numerically investigated in this paper. Two casting directions (i.e., parallel and perpendicular to the longitudinal direction of the beams) and two casting positions (i.e., at the middle and end of the beams) of the pouring outlet are modeled. The flow of fresh and flowable ECC during the casting process is simulated by adopting the 3D SPH modeling [23]. When the casting processes are completed, fiber orientations with the longitudinal direction at different sections of beams are determined for comparison. Moreover, the distribution of fiber orientations regarding different casting techniques is also evaluated and discussed.

2 Modeling of the casting process of ECC beams

2.1 Rheology model

The casting of flowable ECC beam is a process of fresh materials flowing from their dropped place under the funnel outlet to the other parts of formworks. This can be considered as a free-surface flow of a viscous fluid. As a flowable viscous material, its flow behavior can be classified as a Newtonian or non-Newtonian fluid. However, it is practical to treat flowable ECC as a non-Newtonian fluid since the relationship between its shear stress and shear rate is nonlinear, and its effective viscosity varies with time and rate of deformation [20,25]. Moreover, the non-Newtonian fluids have yield stress, which controls the initial stage of the flow. In this regard, the fluid only starts to flow once the yield stress τ_y is exceeded, and when the shear stress falls below the yield stress, the fluid stops flowing. These relationships are expressed in Eqs. (1) and (2) as:

$$\tau = \tau_y + \mu\dot{\gamma} \text{ for } \tau > \tau_y, \tag{1}$$

$$\mu_{\text{eff}} = \frac{\mu_0 + K\dot{\gamma}\mu_\infty}{1 + K\dot{\gamma}}, \tag{2}$$

where μ_{eff}, μ_0, and μ_∞ are the effective viscosity, viscosity at very low and very high shear strain rate $\dot{\gamma}$, respectively, and K is a constant parameter [26].

In the experimental approach, the plastic viscosity and yield stress of fresh cement-based materials are measured using rheometers. However, different rheometers or measured times provide different results of these two parameters [27,28]. Moreover, incorporating fibers in flowable concrete would make obtaining reliable values of these measurements more challenging [29]. Thus, attempts to obtain accurate rheology parameters in the laboratory for modeling input might not be successful. Consequently, several numerical methods have been developed to estimate these two parameters for modeling fresh flowable concrete. In the relevant studies, the yield

stress was first assumed, and then the plastic viscosity was numerically determined [29,30]. This numerical approach was also applied to estimate its yield stress and plastic viscosity for flowable ECC [20].

2.2 Particle-based SPH modeling

Due to the large deformation of flowable ECC during the casting process, the mesh-free or particle-based SPH is a powerful method for solving the governing equations during ECC flow. In SPH, the entire domain of fresh ECC and formwork are modeled by individual particles, including mortar, fiber, and wall-boundary particles. These presented particles generate interactions between mortar, fiber, and the fixed boundary. Also, the synthetic fiber is modeled as inter-connected particles, and thus its two adjacent particles are considered to interact with each other during their movement.

The Lagrangian form of SPH allows tracking the changes in particles' properties during their interaction and motion. At each step of motion, the gradient field variables of a current particle a is approximated by a summation of all surrounding particles b in the support domain Ω of the kernel function W (Fig. 1). The governing equations of a viscous fluid can be written in the SPH forms for flowable ECC as:

$$\frac{\mathrm{d}\rho_a}{\mathrm{d}t} = \sum_b m_b(\boldsymbol{v}_a - \boldsymbol{v}_b)\nabla_a W_{ab}, \tag{3}$$

$$\frac{\mathrm{d}\boldsymbol{v}_a}{\mathrm{d}t} = -\sum_b m_b\left(\frac{P_a}{\rho_a^2} + \frac{P_b}{\rho_b^2}\right)\nabla_a W_{ab} + \boldsymbol{g} + \sum_b m_b\left(\frac{\tau_a}{\rho_a^2} + \frac{\tau_b}{\rho_b^2}\right)\nabla_a W_{ab}, \tag{4}$$

where P, ρ, and t represent the pressure, particle density, and time, respectively. The vector forms of the particle velocity and the gravitational acceleration are denoted by $\boldsymbol{v}$ and $\boldsymbol{g}$, respectively.

As can be seen in Fig. 1, mortar and fiber particles are considered as neighboring particles, and they are included when calculating the forces acting on each other in the support domain Ω. When adding fibers into fresh mortar to produce fresh ECC, plastic viscosity increases due to the interfacial bond between fibers and fresh mortar. Therefore, the SPH method considers fiber particles as passive markers and possessing the same continuum properties as mortar particles. Their motions are mainly governed by the effective viscosity (Eq. (2)), which determines the shear stress tensor τ in Eq. (4) between adjacent particles.

At each time step of the simulation, the velocity and density of mortar and fiber particles are first calculated based on Eqs. (3) and (4). Then, the coordinates of a particle a in three-dimensional space XYZ, i.e., $a(x, y, z)$ are updated based on its previous coordinates. Subsequently, fibers' orientation distributions in a specimen are feasibly evaluated through their coordinates in XYZ space when the casting simulation is completed.

3 Configurations of casting techniques and fiber orientation evaluation

3.1 Initial configurations and parameters

To simulate the casting process of flowable ECC, the boundary particles represented for the funnel and formworks are first created. The position of the funnel outlet and its direction are dependent on the considered casting techniques. Figure 2(a) displays the projection of the funnel outlet in the cases of parallel and perpendicular casting, in which the container of initial materials is located at the middle of beams. As can be seen in Fig. 2(b), the projection of the funnel outlet is perpendicular to the longitudinal beam when two casting positions are studied, i.e., middle-cast and end-cast beams. Then, mortar and synthetic fiber particles are created in a square grid form in the funnels. The volume of container funnels is ensured to be equivalent to the beams' volume. Synthetic fibers are created as straight structures with similar random distribution and orientation at the beginning of the simulations. The distance between the two neighboring particles within a fiber is chosen to equal 2 mm. Using 12 mm length of PVA fibers, a fiber is represented by seven inter-connected particles. Moreover, fiber particles are generated randomly, and their inclination with the longitudinal axis of the beam is in a range of 0° to 90°. The width of the funnel outlet is selected to be equal to 20 mm, which is approximately 1.5 times larger than the length of fibers. This selection allows fibers to freely rotate when they flow through the funnel outlet. Additionally, the beams' formwork height is modeled higher than that of the beams to ensure particles would not spill out during their flow.

The material properties of ECC-M45 in Lepech and Li [31] are utilized as reference data for the simulations. The number of PVA fibers involved in the simulation is determined through its 2% volume in ECC and created mortar particles. The values of two-rheology parameters, including the yield stress $\tau_B = 165$ Pa and the plastics viscosity $\mu_B = 17$ Pa·s, are chosen as in Ref. [20].

3.2 Fiber orientation evaluation

The tensile strain-hardening behavior of ECC is characterized by forming multiple micro-cracks under tension. In practice, these micro-cracks are observed to be approximately perpendicular to the loading direction. Although the crack spacing depends on the stress transfer from bridging fibers at crack planes, the crack spacing in

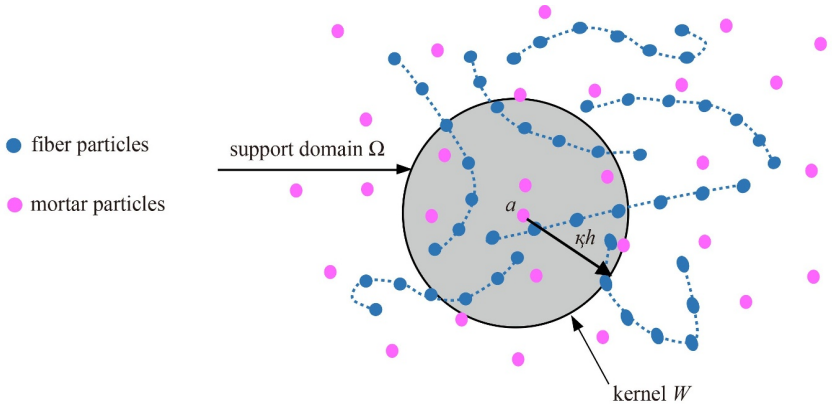

Fig. 1 Fiber, mortar particles and the support domain Ω of the kernel function *W*.

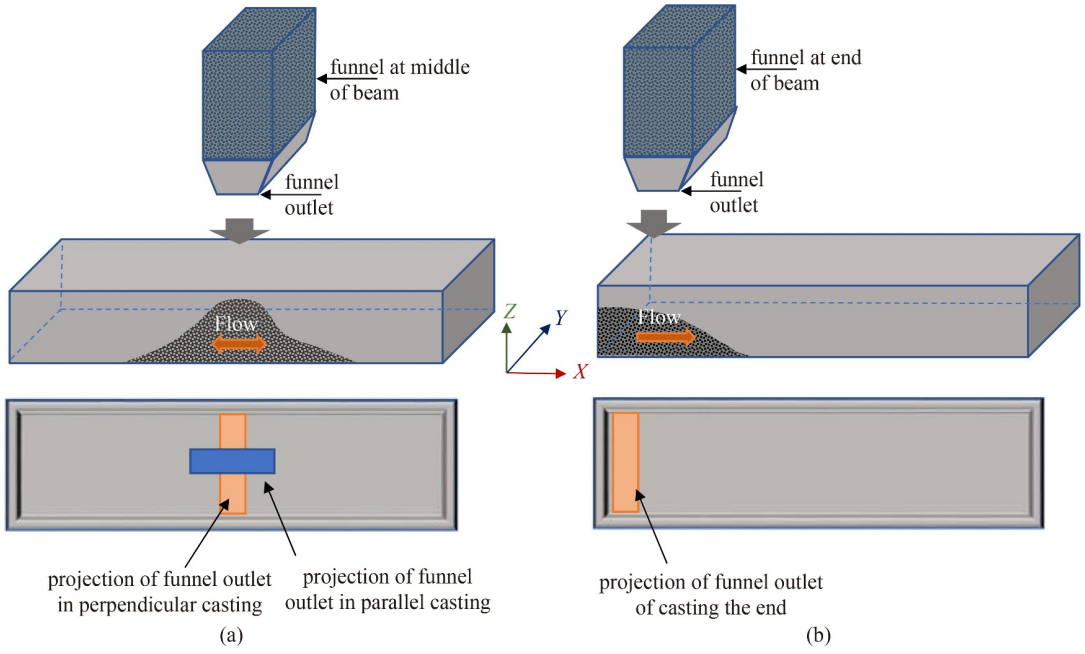

Fig. 2 (a) Perpendicular and parallel casting at the middle of the beam; (b) perpendicular casting at the end of beam.

ECC is typically less than 2 mm [32,33]. These micro-cracks are considered to be flat and perpendicular to the loading axis in the numerical approach. Thus, to evaluate the orientation of fibers at crack planes, beams are virtually cut by multi-vertical planes *ZY* when the casting simulation of beams is completed, as shown in Fig. 3(a). The spacing of cutting planes are chosen to be equal to 2 mm.

Once synthetic fiber particles move along with mortar particles, they become bent during the casting process. Through this bending phenomenon, the distance between two adjacent fiber particles within a fiber when completed casting is always equal or less than their initial assigned distance. Also, a fiber might intersect several cutting *ZY* planes with virtual lines connecting its represented particles, which is illustrated in Fig. 3(b). If two adjacent particles of fiber are fully located between two *ZY* planes, they will not bridge the crack, and thus, their orientation will not be determined. At a *ZY* plane, two inclined angles of an intersected fiber regarding the *XY* and *XZ* planes are trigonometrically calculated via particles' coordinates (x, y, z).

4 Casting simulation, results and discussion

4.1 Perpendicular and parallel casting directions

4.1.1 Casting flow patterns

In this section, two casting directions of the funnel outlet, i.e., perpendicular and parallel directions relative to the longitudinal beam, are modeled. At first, 30625 mortar particles are created in the funnel with the x, y, and z axes spacing equal to 2 mm. Then, the number of fibers is

calculated as 2% of mortar particles (i.e., 2% × 30625 = 613 fibers), which are represented by 4291 fiber particles. These particles are generated to cast a beam of size 13 mm × 60 mm × 350 mm from its center. Figures 4(a) and 4(b) show the obtained flow patterns from two casting directions at three-time steps. During the casting process, mortar and fiber particles drop through the bottom outlet of the funnel to the bottom of the beam below the funnel position, then flow to different parts of the beam. As mortar and fiber particles are assigned to possess identical continuum properties, they flow smoothly together during the casting process. Material particles gradually stop moving after 18 s, and thus the computational modeling for casting simulation is stopped at this time. Additionally, it can be observed that the flow speeds are relatively similar for both casting directions.

4.1.2 Orientation of fibers

The orientation of fibers at cutting planes *ZY* are quantified following the mentioned details in Subsection

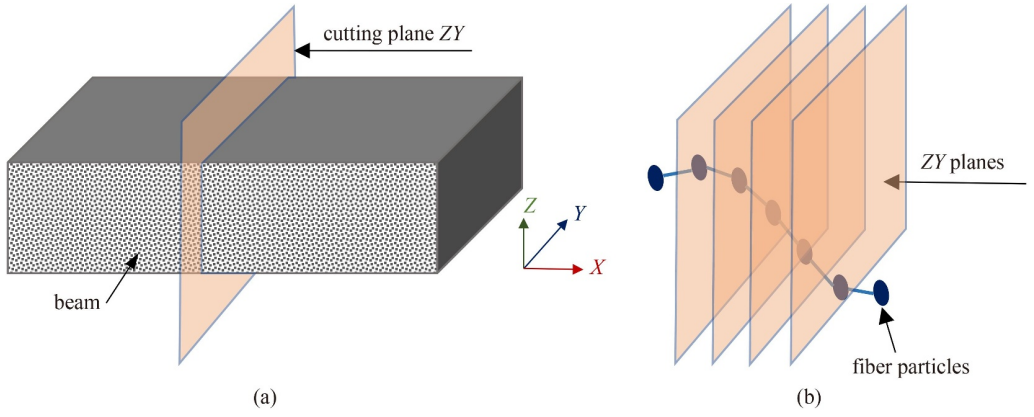

Fig. 3 (a) Cutting a beam with vertical *ZY* planes; (b) fiber intersects several *ZY* planes.

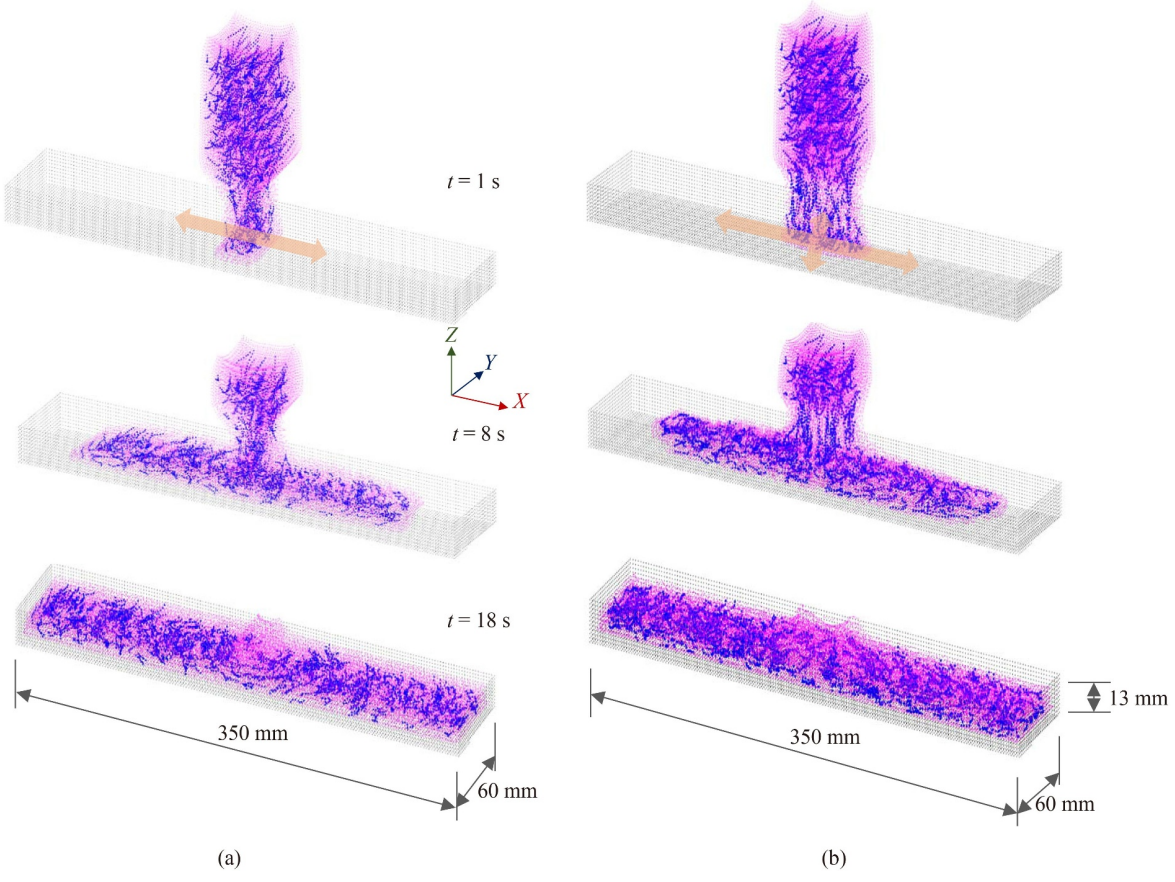

Fig. 4 Casting flow patterns at three-time steps t = 1 s, t = 8 s and t = 18 s: (a) perpendicular casting; (b) parallel casting.

3.2. Figures 5(a) and 5(b) show the 3D view of fiber orientation distributions in two beams. It is observed that more fibers tend to orient parallel with the longitudinal wall in the parallel casting in comparison to the perpendicular casting. This observation can be explained by the flow of fresh ECC in the case of parallel casting pushes fibers toward the longitudinal walls of the beam more strongly than in the case of the perpendicular casting. Therefore, the inclined angles of fibers with respect to the *XZ* plane in the parallel casting case are lower than those in the perpendicular casting, as clearly seen through their polynomial fitting curves in Fig. 6(b). Consequently, while the inclinations of fibers relative to the *XZ* plane noticeably distribute from around 20° to 35° for the parallel casting, whereas a larger number of fibers orientate within the range from 35° to 55° in the perpendicular casting (Fig. 7(b)).

In addition, fibers tend to parallel with the bottom formwork, in which both casting directions attain an average of fiber inclinations with the *XY* plane at around 15°, as illustrated in Fig. 6(a). The reason for this small inclination value is that the 13 mm thickness of the beam in this model causes the 12 mm length of fiber to become more difficult to rotate in almost two-dimensional spaces during their motion. As shown in Fig. 7(a), the differences in fiber orientation distribution with the *XY* plane are insignificant for the two casting directions.

4.2 Casting at the end and middle of beam

4.2.1 Casting flow patterns

To study the influences of casting positions on fiber orientations, two casting processes of the beam of dimensions 100 mm × 100 mm × 350 mm are simulated in which the funnel's positions are at the end and middle of beams. In these models, the thickness of beams is increased to ensure fibers can rotate freely in 3D during their flow. The initial *x*, *y*, and *z* axes spacing of mortar particles in the funnel is also increased to 4 mm to reduce the computational time. This size of beams requires 50688 mortar particles and 7098 fiber particles to represent the fresh ECC. Simulation results at two-time steps of two casting positions are illustrated in Fig.8. Fresh materials flow from one end to another end of the beam in the case of casting at the end. For the middle-cast beam, materials flow from the center of the beam to its ends in two opposite directions.

4.2.2 Orientation of fibers

Figures 9(a) and 9(b) present the 3D view of fiber orientation distribution in two beams when the simulations are completed. It is hard to visually recognize any differences in fiber orientation distribution in two beams of two casting positions from these two figures. For a quantitative assessment, the inclined angles of fibers with *XY* and *XZ* planes for both beams are also determined using the procedure mentioned in Subsection 3.2. As plotted in Fig. 10(a), fibers tend to be parallel with the bottom *XY* plane under the funnel outlet in the end-cast beam (from vertical cross-section 0 to section 40). By contrast, this phenomenon cannot be observed when casting at the middle of the beam. For this reason, the number of fibers inclined with the *XY* plane in the range of 5° to 25° of the end-cast beam is more than that in the case of the middle-cast beam (Fig. 11(a)).

As shown in Fig. 10(b), the inclination of fiber with the *XZ* plane in the middle-cast beam is slightly lower than that of the end-cast beam, except under its funnel outlet area. When casting at the middle, the flow tends to drive

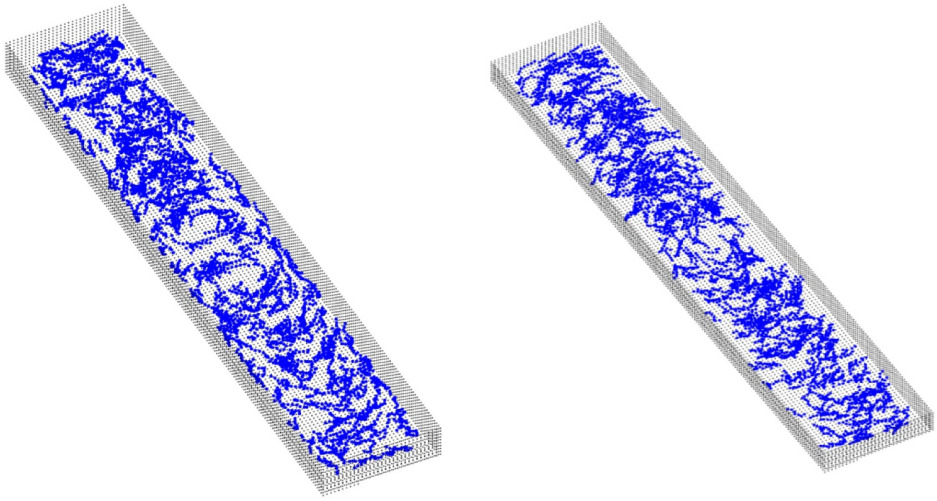

(a) (b)

Fig. 5 The 3D view of fiber orientation distribution in beams when the casting completed: (a) perpendicular casting; (b) parallel casting.

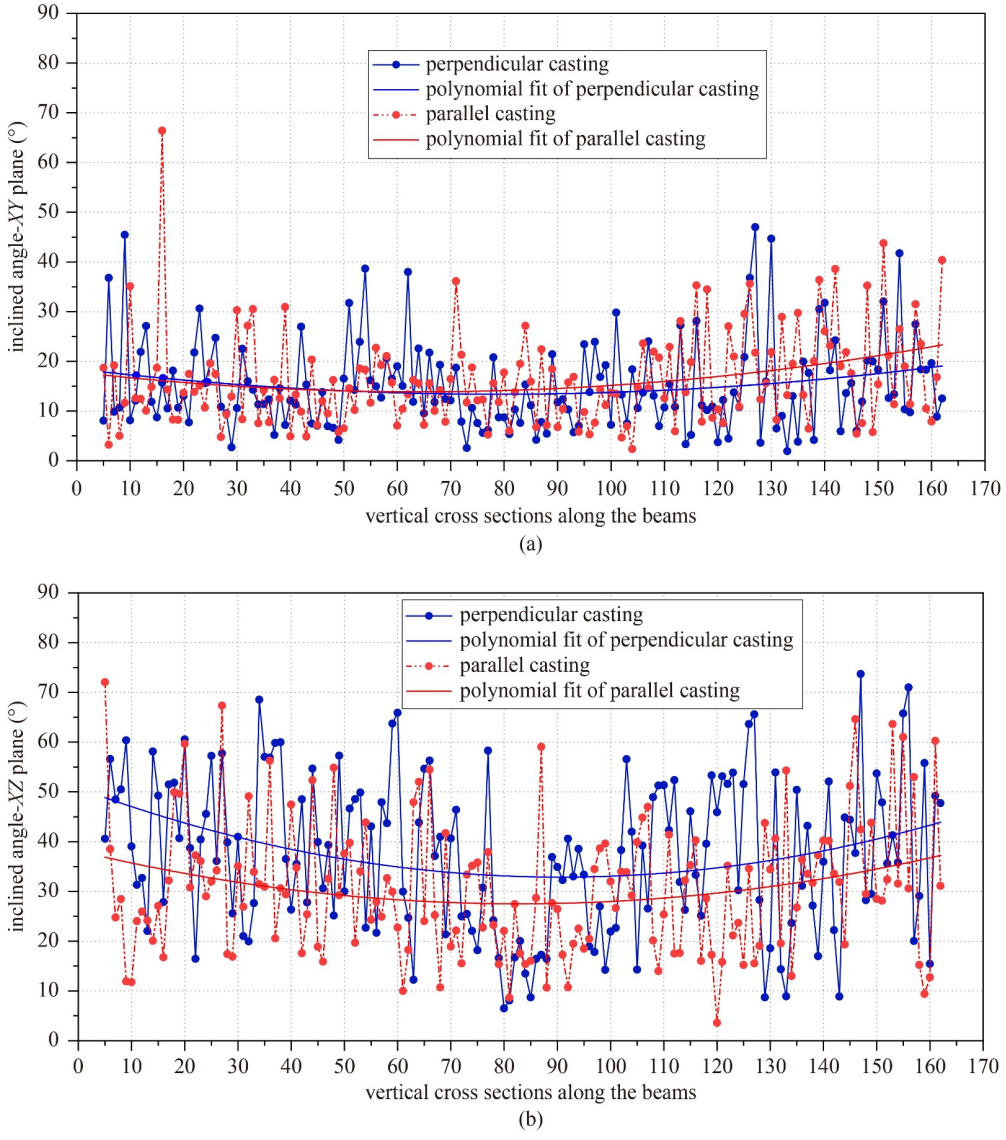

Fig. 6 Orientation of fibers at cutting planes along beams with two casting directions: (a) inclined angle of fibers with *XY* plane; (b) inclined angle of fibers with *XZ* plane.

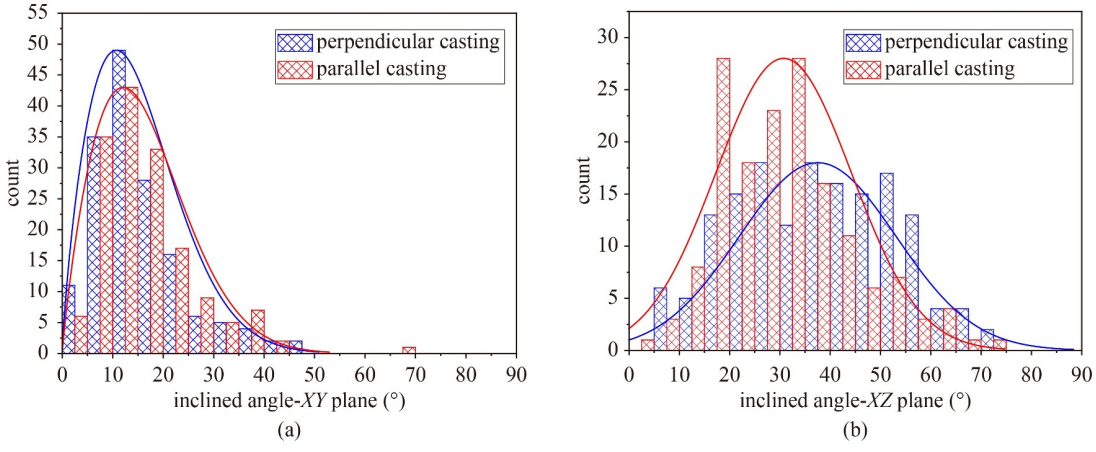

Fig. 7 Distribution of fiber orientation with two casting directions: (a) inclined angle of fibers with *XY* plane; (b) inclined angle of fibers with *XZ* plane.

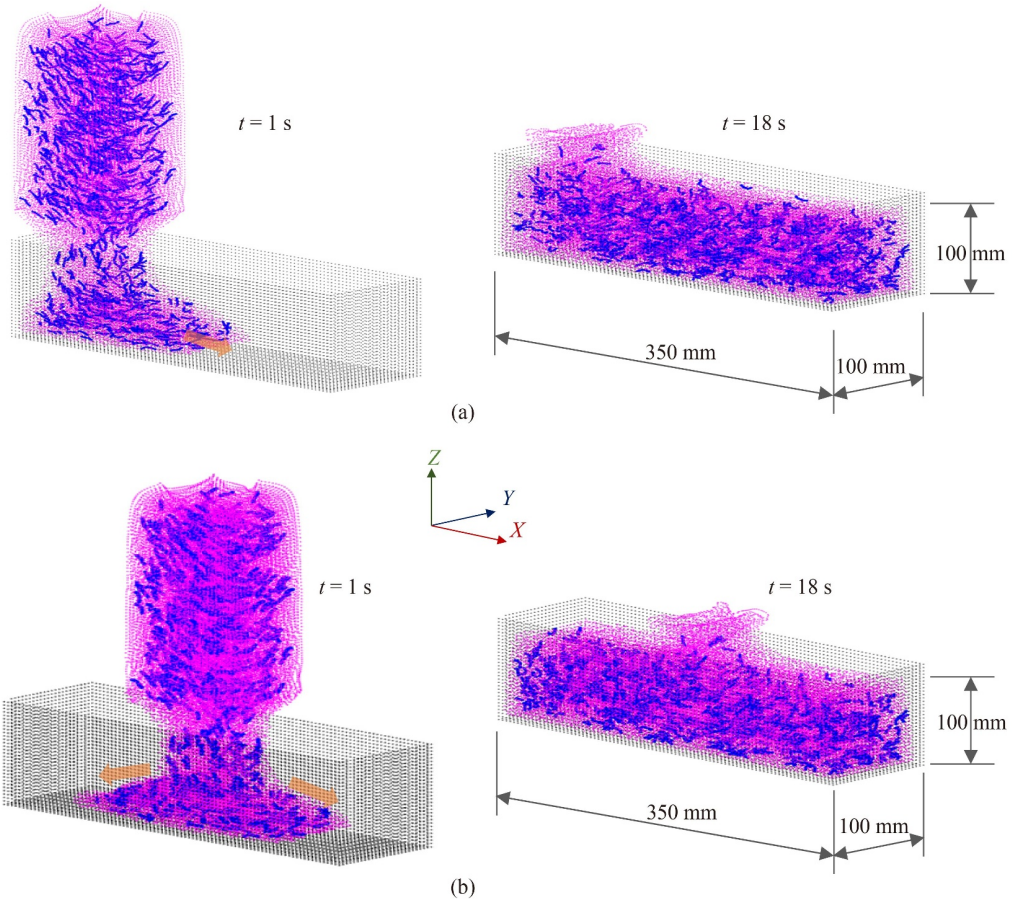

Fig. 8 Flow patterns of casting at the end of beam at two-time steps $t = 1$ s and $t = 18$ s.

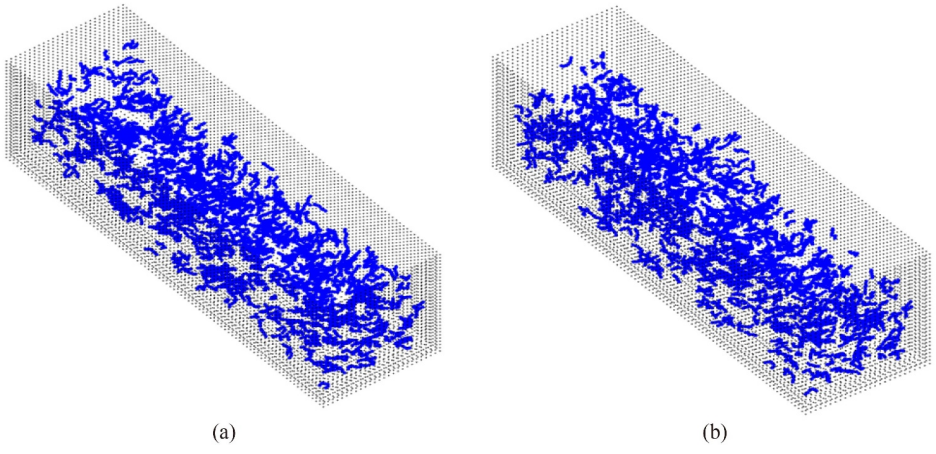

Fig. 9 The 3D view of fiber orientation distribution in beams when the casting is completed: (a) casting at the end of beam; (b) casting at the middle of beam.

fiber toward the two longitudinal walls of the beam more strongly than when casting at the end. As a result, the orientation distribution of fiber with the *XZ* plane in the middle-cast beam, ranging from 25° to 60°, is slightly lower than that in the end-cast beam (Fig. 11(b)). However, the size of the beam might affect the gradient of the flow velocity of different casting positions, which would then influence the flow to induce fiber orientation. Due to the beam dimensions used in these two simulations being narrow and short, the difference in flow velocity might not be noticeable. Therefore, the changes of fiber orientation distributions are negligible, except underneath the pouring position of fresh materials at the funnel outlet.

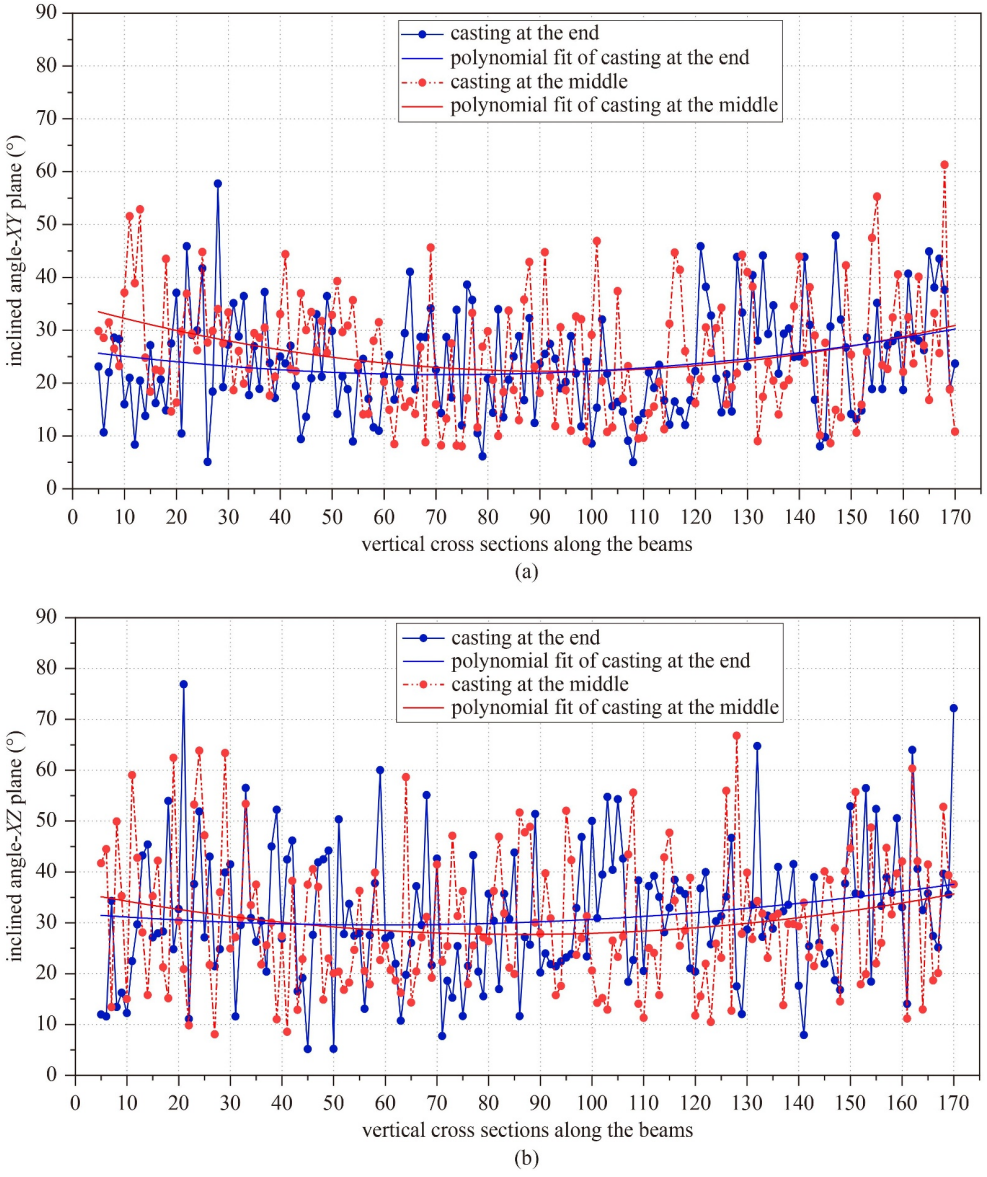

Fig. 10 Orientation of fibers at cutting planes along beams with two casting positions: (a) inclined angle of fibers with *XY* plane; (b) inclined angle of fibers with *XZ* plane.

4.3 Discussion on the fiber orientation distribution and the flexural performance of beams

It is worth mentioning that some other factors might influence the fiber orientation distribution in specimens, such as the manufacturing process or the volume of fibers. First, an inappropriate process to produce fresh ECC could lead to poor dispersion of fibers, which could eventually negatively affect fiber orientation distribution and reduce the efficiency of implemented casting techniques. Therefore, fiber dispersion needs to be controlled throughout the mixing process. It has been shown that adjusting the mixing sequence [34] and rheology control of mortar paste before adding fibers [7] are efficient to achieve better fiber dispersion. Moreover, fiber orientation distribution in beams is expected to vary when the volume/number of fibers is changed. From the experimental point of view, it is impossible to study this variation in the laboratory when changing the volume/number of fibers. In this regard, the numerical simulation in this study is an ideal method to investigate this concern, and it should be conducted in future works.

On the impact of fiber orientation, Ding et al. [10] indicated a significant increase of the ultimate flexural strength and mid-span deflection of beam specimens owning smaller fiber orientation distribution. This experimental result is explained by the increase in bridging stress and complementary energy of smaller inclined fibers when bridging cracks. It is important to note that smaller fiber orientation distribution herein indicates more fibers parallel to the longitudinal direction of the beam, or more fibers perpendicular to flexural

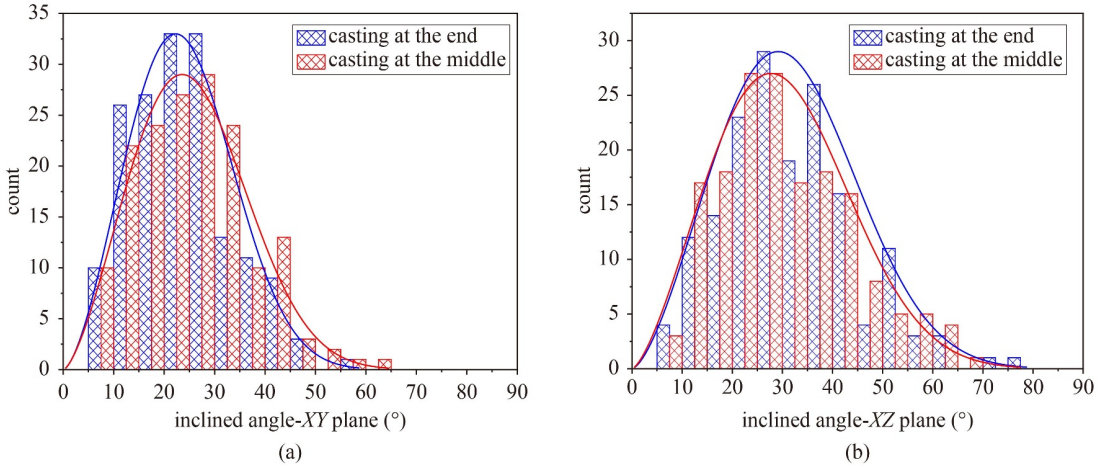

Fig. 11 Distribution of fiber orientation with two casting positions: (a) inclined angle of fibers with *XY* plane; (b) inclined angle of fibers with *XZ* plane.

cracks. By implementing different casting directions, the authors also suggested that the casting direction should be parallel to the loading direction, which maximizes the bridging efficiency of fibers. In this regard, with more fibers that tend to be parallel to the longitudinal walls of the beam, the parallel casting beam in Subsection 4.1 achieves higher flexural strength as it owns lower fiber orientation distribution.

However, the fiber orientation distribution might vary depending on the size of beams and the width of the funnel outlets. On the one hand, fiber orientations might be redistributed when they flow through a narrow funnel outlet. In this regard, fibers can be re-orientated in the anticipated direction by adjusting the size of the outlet. On the other hand, different size of beams cast by flowable fiber reinforced concrete influence their flexural performance [35,36]. Picazo et al. [36] showed that small beams, which exhibited better fiber orientation distribution, achieved higher flexural strength than larger beams. In this current study, the beam 13 mm × 60 mm × 330 mm exhibit the average angle of fiber with *XY* plane is about 15° (Fig. 6(a)), compared to that of around 25° of the 100 mm × 100 mm × 350 mm beam (Fig. 10(a)). This result demonstrates the wall-effect on the rotation of fiber during the casting flow. In small and narrow beams, a larger fiber proportion is restricted in free rotation near the wall boundaries, leading to more fibers parallel with the walls. These fibers contribute to the increase of the flexural strength of small beams compared to larger beams. However, it can be noticed that the flow that induces fiber orientation when casting at different positions has a negligible impact on the fiber orientation distribution of short beams (Fig. 10).

5 Conclusions

The present study numerically evaluates the orientation of fibers in ECC beams considering different casting techniques. Fiber orientations at different cross-sections of beams are observed and evaluated by simulating the casting process of flowable ECC. The results of fiber orientation evaluation considering two casting directions and two casting positions can be presented as follows.

1) The direction of the funnel outlet with the longitudinal beam significantly influences fiber orientation. Fibers tend to be less inclined with the longitudinal walls of beams in the case of parallel casting than in the case of perpendicular casting. Thus, parallel casting in which the funnel outlet parallels with the longitudinal wall of beams is suggested to be implemented to increase the efficiency of fiber in bearing cracks and improving the flexural strength of beams.

2) Fibers have a tendency to become parallel with the bottom of thin beams, regardless of the casting directions. Moreover, thin beam tends to have a smaller fiber inclination with the bottom plane than thick beams.

3) With the short beams in this study, casting positions only slightly affect the fibers' orientation, except for a significantly smaller orientation of fibers with the bottom plane beneath the pouring position when casting at the end of the beam.

Although the obtained results of fiber orientation distribution in this study agree reasonably well with the findings of experimental studies in the literature, future experiments on flowable ECC using synthetic fibers are desirable. The flow-induced fiber orientation might be more significant for longer beams when considering different casting techniques. The flow velocity gradient is also affected by the fresh-state properties of ECC materials. Therefore, different fresh-state properties and longer beams are the two factors that need to be considered in future studies.

Acknowledgements This work belongs to the project No. T2021-97TD in 2021 funded by Ho Chi Minh City University of Technology and Education, Vietnam.

Funding note Open Access funding enabled and organized by CAUL and its Member Institutions.

References

1. Li V C. On engineered cementitious composites (ECC). Journal of Advanced Concrete Technology, 2003, 1(3): 215−230
2. Li V C. Tailoring ECC for special attributes: A review. International Journal of Concrete Structures and Materials, 2012, 6(3): 135−144
3. Li V C, Wu C, Wang S, Ogawa A, Saito T. Interface tailoring for strain-hardening polyvinyl alcohol-engineered cementitious composite (PVA-ECC). Materials Journal, 2002, 99(5): 463−472
4. Yang E H, Wang S, Yang Y, Li V C. Fiber-bridging constitutive law of engineered cementitious composites. Journal of Advanced Concrete Technology, 2008, 6(1): 181−193
5. Kanakubo T, Miyaguchi M, Asano K. Influence of fiber orientation on bridging performance of polyvinyl alcohol fiber-reinforced cementitious composite. ACI Materials Journal, 2016, 113(2): 131−141
6. Ranade R, Stults M, Lee B, Li V. High Performance Fiber Reinforced Cement Composites 6. Berlin: Springer, 2012, 107−114
7. Li M, Li V C. Rheology, fiber dispersion, and robust properties of engineered cementitious composites. Materials and Structures, 2013, 46(3): 405−420
8. Ouyang C, Pacios A, Shah S. Pullout of inclined fibers from cementitious matrix. Journal of Engineering Mechanics, 1994, 120(12): 2641−2659
9. Leung C K, Ybanez N. Pullout of inclined flexible fiber in cementitious composite. Journal of Engineering Mechanics, 1997, 123(3): 239−246
10. Ding C, Guo L, Chen B. Orientation distribution of polyvinyl alcohol fibers and its influence on bridging capacity and mechanical performances for high ductility cementitious composites. Construction & Building Materials, 2020, 247: 118491
11. Lu C, Leung C K. Theoretical evaluation of fiber orientation and its effects on mechanical properties in Engineered Cementitious Composites (ECC) with various thicknesses. Cement and Concrete Research, 2017, 95: 240−246
12. Zhou B, Uchida Y. Influence of flowability, casting time and formwork geometry on fiber orientation and mechanical properties of UHPFRC. Cement and Concrete Research, 2017, 95: 164−177
13. Ferrara L, Ozyurt N, Di Prisco M. High mechanical performance of fibre reinforced cementitious composites: The role of "casting-flow induced" fibre orientation. Materials and Structures, 2011, 44(1): 109−128
14. Huang H, Su A, Gao X, Yang Y. Influence of formwork wall effect on fiber orientation of UHPC with two casting methods. Construction & Building Materials, 2019, 215: 310−320
15. Qiao Z, Pan Z, Xue W, Meng S. Experimental study on flexural behavior of ECC/RC composite beams with U-shaped ECC permanent formwork. Frontiers of Structural and Civil Engineering, 2019, 13(5): 1271−1287
16. Abbas A A, Arna 'Ot F H, Abid S R, Özakça M. Flexural behavior of ECC hollow beams incorporating different synthetic fibers. Frontiers of Structural and Civil Engineering, 2021, 15(2): 399−411
17. Deeb R, Karihaloo B, Kulasegaram S. Reorientation of short steel fibres during the flow of self-compacting concrete mix and determination of the fibre orientation factor. Cement and Concrete Research, 2014, 56: 112−120
18. Huang H, Gao X, Li Y, Su A. SPH simulation and experimental investigation of fiber orientation in UHPC beams with different placements. Construction & Building Materials, 2020, 233: 117372
19. Bi J, Bao C, Xu D, Guan J, Cheng W. Numerical simulation of the distribution and orientation of steel fibres in the SCC. Magazine of Concrete Research, 2017, 69(16): 811−822
20. Thanh H T, Li J, Zhang Y X. Numerical modelling of the flow of self-consolidating engineered cementitious composites using smoothed particle hydrodynamics. Construction & Building Materials, 2019, 211: 109−119
21. Deeb R, Kulasegaram S, Karihaloo B L. 3D modelling of the flow of self-compacting concrete with or without steel fibres. Part II: L-box test and the assessment of fibre reorientation during the flow. Computational Particle Mechanics, 2014, 1(4): 391−408
22. Švec O, Skoček J, Stang H, Geiker M R, Roussel N. Free surface flow of a suspension of rigid particles in a non-Newtonian fluid: A lattice Boltzmann approach. Journal of Non-Newtonian Fluid Mechanics, 2012, 179: 32−42
23. Thanh H T, Li J, Zhang Y X. Numerical simulation of self-consolidating engineered cementitious composite flow with the V-funnel and U-box. Construction & Building Materials, 2020, 236: 117467
24. Tran Thanh H , Li J, Zhang Y. Numerical evaluation the effect of specimen thickness on fibre orientation in self-consolidating engineered cementitious composites. In: RILEM-fib International Symposium on Fibre Reinforced Concrete. Valencia: Springer, 2020
25. Kulasegaram S, Karihaloo B L. Fibre-reinforced, self-compacting concrete flow modelled by smooth particle hydrodynamics. Proceedings of the Institution of Civil Engineers-Engineering and Computational Mechanics, 2013, 166(1): 22−31
26. Shao S, Lo E Y M. Incompressible SPH method for simulating Newtonian and non-Newtonian flows with a free surface. Advances in Water Resources, 2003, 26(7): 787−800
27. Ferrara L, Cremonesi M, Tregger N, Frangi A, Shah S P. On the

identification of rheological properties of cement suspensions: Rheometry, computational fluid dynamics modeling and field test measurements. Cement and Concrete Research, 2012, 42(8): 1134−1146

28. Kostrzanowska-Siedlarz A, Gołaszewski J. Rheological properties of high performance self-compacting concrete: Effects of composition and time. Construction & Building Materials, 2016, 115: 705−715
29. Ghanbari A, Karihaloo B L. Prediction of the plastic viscosity of self-compacting steel fibre reinforced concrete. Cement and Concrete Research, 2009, 39(12): 1209−1216
30. Lashkarbolouk H, Halabian A M, Chamani M R. Simulation of concrete flow in V-funnel test and the proper range of viscosity and yield stress for SCC. Materials and Structures, 2014, 47(10): 1729−1743
31. Lepech M D, Li V C. Large-scale processing of engineered cementitious composites. ACI Materials Journal, 2008, 105(4): 358−366
32. Wang S, Li V C. Polyvinyl alcohol fiber reinforced engineered cementitious composites: Material design and performances. In: Proceedings of International RILEM Workshop on HPFRCC in Structural Applications. Hawaii: Citeseer, 2005
33. Şahmaran M, Li V C. Durability properties of micro-cracked ECC containing high volumes fly ash. Cement and Concrete Research, 2009, 39(11): 1033−1043
34. Zhou J, Qian S, Ye G, Copuroglu O, van Breugel K, Li V C. Improved fiber distribution and mechanical properties of engineered cementitious composites by adjusting the mixing sequence. Cement and Concrete Composites, 2012, 34(3): 342−348
35. Nguyen D L, Kim D J, Ryu G S, Koh K T. Size effect on flexural behavior of ultra-high-performance hybrid fiber-reinforced concrete. Composites. Part B, Engineering, 2013, 45(1): 1104−1116
36. Picazo Á, Alberti M G, Gálvez J C, Enfedaque A, Vega A C. The size effect on flexural fracture of polyolefin fibre reinforced concrete. Applied Sciences (Basel, Switzerland), 2019, 9(9): 1762